High repetition-rate frequency combs without modelocking

by

Daniel C. Cole

B.S., Washington University in St. Louis, 2012

A thesis submitted to the

Faculty of the Graduate School of the

University of Colorado in partial fulfillment

of the requirements for the degree of

Doctor of Philosophy

Department of Physics

2018

This thesis entitled:
High repetition-rate frequency combs without modelocking
written by Daniel C. Cole
has been approved for the Department of Physics

_____

Reader1

_____

Reader2

Date _____

The final copy of this thesis has been examined by the signatories, and we find that both the content and the form meet acceptable presentation standards of scholarly work in the above mentioned discipline.

Cole, Daniel C. (Ph.D., Physics)

High repetition-rate frequency combs without modelocking

Thesis directed by Dr. Scott A. Diddams

Optical frequency combs based on modelocked lasers have revolutionized precision metrology by enabling measurements of optical frequencies, with implications both for fundamental scientific questions and for applications such as fast, broadband spectroscopy. In this thesis, I describe advances in the generation of frequency combs without modelocking in platforms with smaller footprints and higher repetition rates, with the ultimate goal of bringing frequency combs to new applications in a chip-integrated package. I discuss two approaches for comb generation: parametric frequency conversion in Kerr microresonators and active electro-optic modulation of a continuous-wave laser. After introducing microresonator-based frequency combs (microcombs), I discuss two specific developments in microcomb technology: First, I describe a new, extremely reliable method for generation of soliton pulses through the use of a phase-modulated pump laser. This technique removes the dependence on initial conditions that was formerly a universal feature of these experiments, presenting a solution to a significant technical barrier to the practical application of microcombs. Second, I present observations of 'soliton crystal' states with highly structured 'fingerprint' optical spectra that correspond to ordered pulse trains exhibiting crystallographic defects. These pulse trains arise through interaction of solitons with avoided mode-crossings in the resonator spectrum. I also discuss generation of Kerr soliton combs in the Fabry-Perot (FP) geometry, with a focus on the differences between the FP geometry and the ring geometry that has been the choice of most experimenters to date. Next, I present results on combs based on electro-optic modulation. I discuss the operational principle, and then describe the first self-referencing of a frequency comb based on active modulation and a proof-of-principle metrology experiment. Finally, I discuss a technique for reducing the repetition rate of a high-repetition-rate frequency comb, which will be a necessary post-processing step for some applications. I conclude with a discussion of avenues for future research.

Acknowledgements

The work in this thesis would not have been possible...

- Acknowledgement line 1
- Acknowledgement line 2

Contents

Figures

Chapter 1

EOM Combs

In this chapter, I discuss the generation of high-repetition-rate frequency combs through electro-optic modulation of a continuous-wave laser—so-called EOM combs [96–105]. This scheme represents an alternative to parametric generation of high-repetition-rate combs in Kerr resonators, and as the technology matures it will likely find a niche in the application space that leverages its long-term stability, lack of moving parts, and possibility for robust turn-key operation. First I present the operational principle, followed by experimental results that represent the first $f-2f$ self-referencing of a comb of this kind. Then I provide a discussion of the noise processes specific to the EOM comb, the investigation and mitigation of which is a significant contribution of the work described here. I conclude with a brief outlook for the technology.

1.1 Principle of operation

At its simplest, an EOM comb is a set of lines generated by passing a CW 'seed' laser through cascaded phase and intensity modulators to generate a train of chirped pulses. After this initial step, the pulse train may be propagated through a dispersive medium to temporally compress the pulses, and they can be subsequently spectrally broadened. A generic expression for the electric field before temporal compression results from the product of the field $E_o e^{-i\omega_c t}$ with operators

$$\frac{e^{i\Phi(t)} + e^{-i\Phi(t)}}{2} = \cos\Phi(t) \tag{1.1}$$

where

$$\Phi(t) = \phi_{DC} + \phi_{RF}\sin\left(\omega_{rep}t + \phi_{IMPM}\right) \tag{1.2}$$

representing the intensity modulation and

$$\exp\left[i\delta_{PM}\sin\omega_{rep}t\right] \tag{1.3}$$

representing the phase modulation. Here E_o and ω_c are the complex amplitude and the carrier frequency of the seed laser. The phases ϕ_{DC} and ϕ_{RF} represent the DC bias and depth of the intensity modulation, respectively, which experimentally are sourced from a DC power supply and an RF synthesizer. Writing the intensity-modulation operator as the sum of exponentials reveals the physical origin of intensity modulation as phase modulation in two paths with opposite sign. The phase-modulation index, which sets the initial bandwidth of the EOM comb, is δ_{PM}. The comb's repetition rate is $f_{rep} = \omega_{rep}/2\pi$, with ω_{rep} the angular frequency of the phase and intensity modulation. In practice it is useful to derive these signals from the same synthesizer. The phase ϕ_{IMPM} represents a phase difference between the IM and PM operators arising from path-length differences, which can be controlled via the insertion of a phase shifter in one electrical path.

For convenient temporal pulse compression and subsequent spectral broadening of the comb it is desirable to configure the IM and PM to yield a train of 50 % duty-cycle pulses with normal chirp (temporally increasing carrier frequency). To achieve this, both ϕ_{DC} and ϕ_{RF} are set to $\pi/4$ and ϕ_{IMPM} is set to zero. Experimentally, one can determine that the appropriate RF drive power

and bias have been applied by adjusting the ratios $\eta_1 = P_1/P_0$ and $\eta_2 = P_2/P_0$ between the first- and second-order sidebands and the carrier to $\eta_1 = -7.4$ dB and $\eta_2 = -21.3$ dB with only intensity modulation applied to the seed laser.[1] Setting ϕ_{IMPM} to either zero or π is achieved by examining the optical spectrum of the EOM comb with both IM and PM applied. The spectrum is asymmetric if ϕ_{IMPM} is not zero or π due to stronger transmission of either the high- or low-frequency components of the phase-modulated seed laser through the intensity modulators. The optical spectrum of the comb, which does not include phase information, is the same for $\phi_{IMPM} = 0$ or π; the difference between the two corresponds to reversal of the field in time or, equivalently, the difference between normal and anomalous chirp. Setting ϕ_{IMPM} to zero is accomplished by verifying that the pulses are compressed by propagation in an appropriate length of an anomalously dispersive medium; $\phi_{IMPM} = \pi$ corresponds to anomalous chirp on the initial pulse train, in which case the pulses will not be compressed.

A simplified and illuminating expression for the electric field of a normally-chirped 50 % duty-cycle pulse train (up to a constant overall phase shift relative to the previous expression) is:

$$E = E_o \cos\left(\frac{\pi}{2}\sin^2\frac{\omega_{rep}t}{2}\right) e^{i\omega_c t - i\delta_{PM}\cos\omega_{rep}t}. \tag{1.4}$$

This can be understood as the product of a time-varying real amplitude $a(t) = E_o \cos\left(\frac{\pi}{2}\sin^2\frac{\omega_{rep}t}{2}\right)$ and a phase factor from which the instantaneous carrier frequency $\omega(t) = \omega_c + \omega_{rep}\delta_{PM}\sin\omega_{rep}t$ can be calculated. The carrier frequency $\omega(t)$ is increasing when the amplitude $a(t)$ is at its maximum, corresponding to normal chirp on the pulses.

1.2 Generation of an EOM comb and detection of its carrier-envelope offset frequency

Here I describe the generation of an EOM comb with 10 GHz repetition rate and subsequent measurement of its carrier-envelope offset frequency. One advantage of the EOM comb scheme is that the generation and spectral broadening of the comb is well understood, and can be modeled accurately. To demonstrate this, I compare the results of simulations of the comb to the experimental output at each stage in the generation process.

The experimental setup is depicted in Fig. 1.1a. The basic experimental scheme consists of the following steps: 1. Initial generation and temporal compression of the EOM comb pulse train; 2. Modest spectral broadening and temporal re-compression; 3. Noise reduction using a Fabry-Perot filter cavity; and 4. Octave-spanning supercontinuum generation and detection of the carrier-envelope offset frequency. To my knowledge, the results described below represent the first time a frequency comb of this kind has been self-referenced. Key to the success of this approach is the implementation of nonlinear spectral broadening in two stages, which allows the second stage to be seeded with ∼130 fs pulses for coherent supercontinuum generation. Noise reduction with the Fabry-Perot filter cavity is also critical for coherent spectral broadening; I describe a characterization of this step below.

To generate the initial train of chirped pulses, a telecommunications-band CW laser is passed through cascaded phase and intensity modulators driven with a 10 GHz microwave signal. The intensity modulator is biased at the 50 % transmission point and driven with an RF amplitude appropriate for generation of a 50 % duty-cycle pulse train, as described above; the phase modulator is driven with modulation depth of $\sim 31\pi/4 \sim 24.3$ rad. The relative phase between the modulators

[1] This assumes that the modulation is applied to both paths in the intensity modulator with opposite sign; the correct ratios for a Mach-Zehnder intensity modulator with modulation in only one path are $\eta_1 = -5.8$ dB and $\eta_2 = -12.9$ dB. This difference arises from residual phase modulation on the output field in the latter case. To determine the internal configuration of the modulator, one can examine the action of the bias: if the modulation is applied to both paths with opposite signs, the bias will adjust only the ratios between the odd- and even-order sidebands while leaving the ratios within each group fixed. However, if the modulation is applied to only one path, the bias will change the ratio of each sideband to the carrier. These conclusions are reached by application of various forms of the Jacobi-Anger expansion.

is set such that the phase applied by the phase modulator is at a minimum when the transmission of the intensity modulator is highest; this yields a train of normally-chirped (up-chirped) pulses. Simulated temporal intensity and instantaneous carrier-frequency profiles are shown in Fig. 1.1b, and a simulated optical spectrum is overlaid on an experimental measurement in Fig. 1.1c.

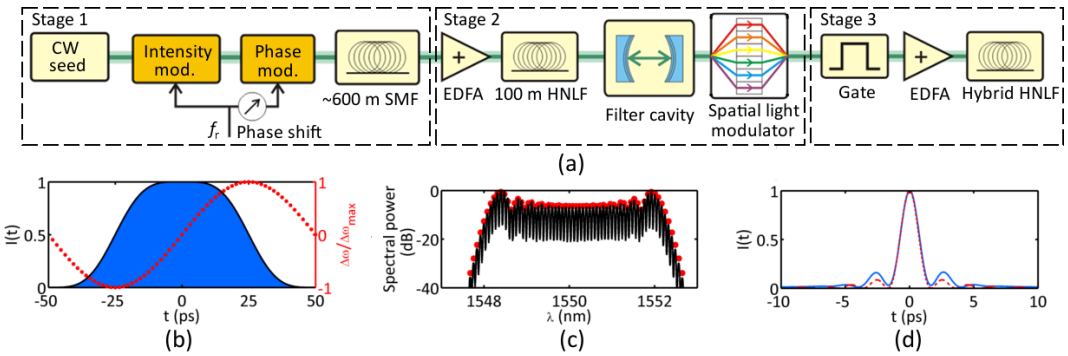

Figure 1.1: **Schematic and principle of operation for generation of a coherent octave-spanning EOM comb supercontinuum.** (a) Experimental schematic for supercontinuum generation, with three stages: 1. Initial generation and temporal compression of the pulse train; 2. First stage of spectral broadening and temporal re-compression, along with a filter cavity for noise suppression, and 3. Final stage of spectral broadening for generation of a coherent octave-spanning supercontinuum, including the implementation of an electro-optic gate for repetition-rate downsampling. (b) Depiction of a constituent pulse from a train of 50 % duty-cycle normally-chirped pulses with 10 GHz repetition rate. Intensity is shown in blue, and instantaneous carrier frequency is shown in red. The periodic electric field of this pulse train is given by Eqn. 1.4. (c) Measured optical spectrum of the initial EOM comb pulse train (black), along with the simulated spectrum corresponding to the plots in panel (b). (d) Simulated temporal compression of the pulses shown in panel (b), with compression conducted by propagation in 570 m of SMF (solid blue) and compression to the transform limit (dashed red). The full-width at half-maximum (FWHM) duration of both pulses is ∼1.5 ps.

Next, the chirped pulse train is propagated through 600 m of anomalously-dispersive SMF. The length of SMF that is appropriate for pulse compression depends on the bandwidth of the optical pulses to be compressed; equivalently, it depends on both the phase-modulation depth and the repetition rate of the pulse train. This temporal compression reduces the duration of the optical pulses from ∼50 ps to ∼ 1.5 ps. A simulation of the resulting intensity profile is presented in Fig. 1.1d.

The compressed pulses are amplified to 400 mW average power in an erbium-doped fiber amplifier and launched into 100 m of HNLF. This section of HNLF has chromatic dispersion that is small and normal; this is carefully chosen to chirp the pulses via self-phase modulation while avoiding soliton-fission dynamics[106]. The result is a train of chirped ∼1.5 ps pulses exiting the fiber. In Fig. 1.2a we present the measured optical spectrum of this pulse train, as well as results of a numerical simulation of the spectral broadening in the 100 m of normally-dispersive HNLF. These simulations are conducted using the nonlinear Schrodinger equation (NLSE) including third order dispersion[27], taking as initial conditions the calculated intensity profile of the EOM comb pulses shown in Fig. 1.1d. The dispersion values for the HNLF used in the simulation are $D = -0.04$ ps/nm·km and $D' = 0.003$ ps/nm^2·km, close to the values specified by the manufacturer. The simulation method is described in detail in App. A.

After propagation through the first section of HNLF, the pulses are passed through a high-finesse Fabry-Perot cavity for suppression of optical frequency fluctuations as discussed below. Then the pulses are temporally compressed again, this time using a commercial spatial light modulator

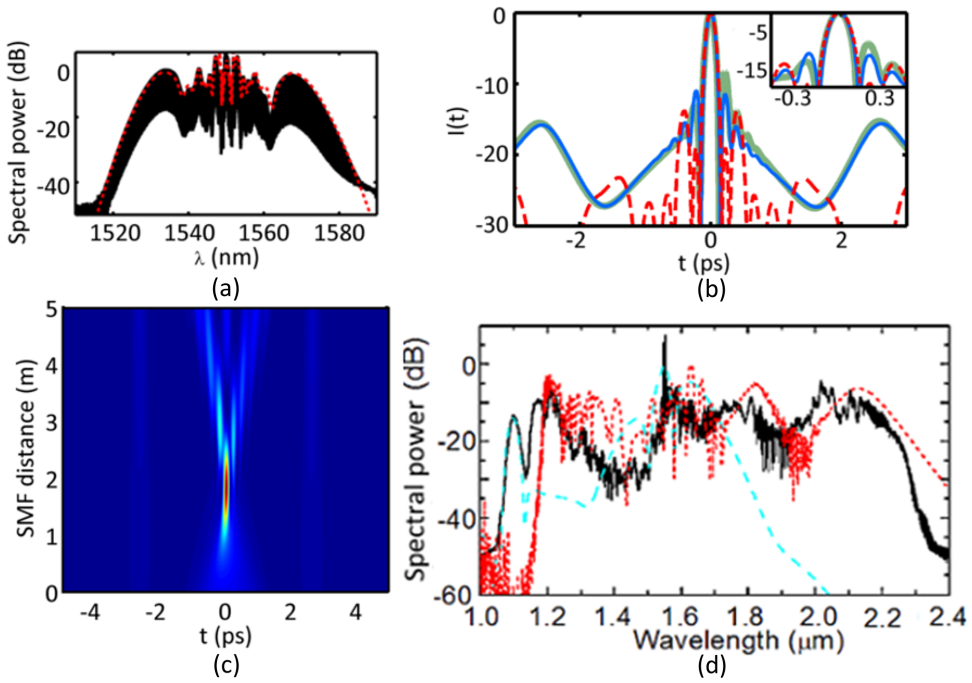

Figure 1.2: **Spectral broadening for generation of an octave-spanning supercontinuum.** (a) Measured optical spectrum after propagation in 100 m of low-normal-dispersion HNLF (black). The spectrum is broadened by self-phase modulation, which imposes a chirp on the pulses. Shown in red is a simulation of the same, conducted as described in the text. (b) Logarithmic-scale plot of the simulated pulse intensity envelopes after temporal recompression in the SLM with 2^{nd}-, 3^{rd}-, and 4^{th}-order dispersion (blue), in an appropriate length of SMF (thick green), to the transform limit (dashed red). (c) Simulated re-compression of the SPM-chirped pulses (red spectrum in panel (a)) in SMF. (d) Measured optical spectrum of the octave-spanning supercontinuum generated by the EOM comb system (black), plotted along with simulated spectra calculated as described in the text to investigate the effects of the 30 cm, highly-dispersive piece of HNLF (long-dashed teal) and the 7.7 m, lower-dispersion piece of HNLF (short-dashed red).

(SLM) [107]; the SLM separates narrow spectral regions using a grating and passes them through individually controlled delaying elements before recombination. The SLM applies 2^{nd}, 3^{rd}, and 4^{th} order chromatic dispersion, which simulations indicate is sufficient to compress the chirped pulses to ∼130 fs, near their transform limit. This is shown in Fig. 1.2b. While it is convenient, the SLM is not strictly necessary; it would also be possible to compress the pulses via propagation in an appropriate length of SMF. Figs. 1.2b and c present the output intensity profile and the evolution of the intensity profile, respectively, in simulated compression in SMF. Because the pulses are broadband, temporally short, and reasonably high energy, these simulations include the full dispersion profile of SMF and the Kerr nonlinearity.

The temporally compressed ∼130 fs pulses are then passed through a Mach-Zehnder modulator functioning as an electro-optic gate for repetition-rate downsampling (see Chapter **??**). The gate selectively transmits every fourth pulse, reducing the repetition rate of the pulse train to 2.5 GHz. This facilitates coherent supercontinuum generation in a second stage of spectral broadening by increasing the pulse energy that can be achieved at a given average power. Note that this step is convenient but not strictly necessary, as shown in Ref. [108].

The downsampled 2.5 GHz pulse train is amplified to an average power of 1.4 W, resulting in a train of ∼0.56 nJ pulses. This pulse train is propagated through 8 m of hybrid HNLF, yielding

the spectrum shown in Fig. 1.2d. This hybrid HNLF consists of two segments with different dispersion profiles, with each segment serving a different purpose. The first segment is 30 cm long and highly dispersive (D = 6 ps/nm·km), and generates a dispersive wave centered at 1090 nm. The second segment is 7.7 m long and has lower dispersion (D = 1.5 ps/nm·km), and generates a Raman-self-frequency-shifted soliton centered near 2150 nm. The effect of each of these fibers on the output spectrum can be understood by investigating propagation in each section separately. To do this we use the LaserFOAM program [109], which employs the generalized NLSE including Raman scattering, self-steepening, and 2nd- through 4th-order dispersion. The simulations are run independently, and both take as their initial conditions 170 fs Gaussian pulses with 350 pJ energy, close to the energy coupled into the HNLF after accounting for losses. The results of these simulations are plotted in Fig. 1.2d.

The supercontinuum generated in the hybrid HNLF is coherent and suitable for $f-2f$ self-referencing. To detect the carrier-envelope offset frequency of the EOM comb, we pass the pulse train through an interferometer consisting of a dichroic mirror, a delay stage in one path, and a 10 mm sample of periodically-poled lithium niobate that generates the second harmonic of supercontinuum light at 2140 nm. The dichroic mirror and delay stage enable adjustment of the relative timing between the native 1070 nm and doubled 2140 nm components of the supercontinuum so that they are temporally coincident. An optical band-pass filter centered at 1070 nm selects the supercontinuum components required for self-referencing, shown in Fig. 1.3a, and impinging the filtered light on a photodetector reveals the carrier-envelope offset frequency of the EOM comb, shown in Fig. 1.2b. Note that downsampling introduces an ambiguity in the offset frequency due to the increased density of comb modes in the downsampled pulse train; this ambiguity can be removed by measuring the change in measured offset frequency with a change in $f_{rep} = \omega_{rep}/2\pi$ provided by the synthesizer driving the modulators.

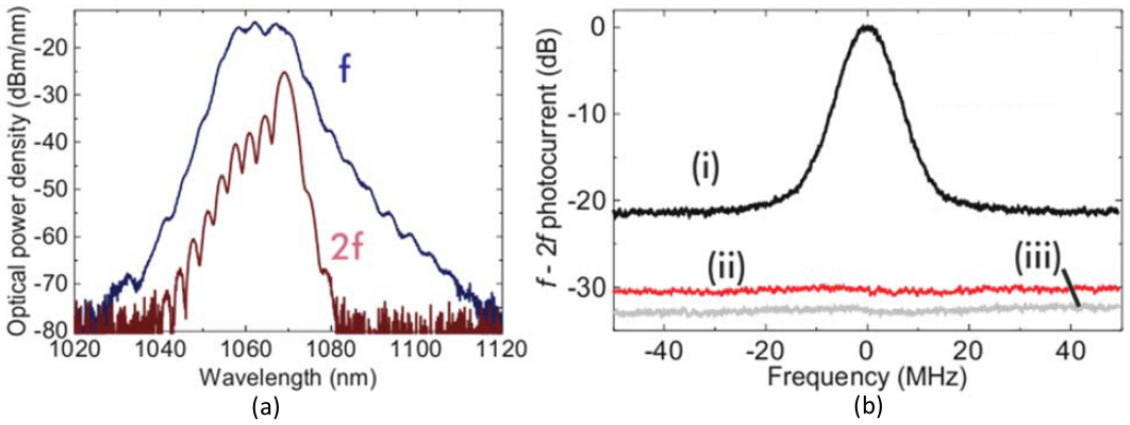

Figure 1.3: **Self-referencing of an EOM comb.** (a) Spectral components used for $f-2f$ self-referencing after passing through a 1070-nm optical bandpass filter: native supercontinuum light (blue) and frequency-doubled 2140-nm supercontinuum light (red) ARE THESE LABELED CORRECTLY. (b) Photodetected carrier-envelope offset frequency signal (black), along with a measurement of the intensity noise of the pulse train obtained by blocking one of the paths (red) and the photodetector noise floor (grey). The intensity-noise measurement highlights the presence of a broad background noise floor on the f_0 signal that must be the result of frequency fluctuations because it is not present when photodetecting either path alone.

1.3 Noise considerations in EOM comb generation

An important difference between the EOM comb scheme and other approaches for generation of frequency combs is that the repetition rate is derived from a microwave source and is multiplied directly by a factor μ to yield the frequency-comb mode with seed-laser-referenced mode number μ. Therefore, the contribution to the frequency noise of mode μ from the microwave source scales with the μ, and the contribution to the power spectrum of frequency noise scales as μ^2. This presents a challenge in the generation of coherent supercontinuum light, where the modes relevant for $f-2f$ self-referencing are far from the seed laser and μ is large. The factor by which the noise on the modulation tone f_{rep} is multiplied to determine its contribution to the noise on the measured carrier-envelope offset frequency is the ratio between the comb's carrier frequency (the frequency of the seed laser) and the repetition rate: $\mu = f_c/f_{rep}$ =19340 for the 10 GHz comb discussed above (where f_c =193.4 THz for a 1550 nm seed laser). This contribution is shown in Fig. 1.4a, along with the contribution from the CW seed laser. The noise on f_{rep} results from technical noise on the synthesizer tone at low Fourier frequencies and approaches a white Johnson-Nyquist (thermal) phase-noise floor of -177 dBm/Hz at high Fourier frequencies. Noise in each of these regimes impacts the photodetected f_0 signal: low-frequency noise contributes to the linewidth of the comb modes and therefore the f_0 signal, while high-frequency noise contributes to a frequency-noise floor on the photodetected signal[110]. Unmitigated multiplication of this noise floor by the factor μ^2 =19340^2 leads to a supercontinuum with optical frequency fluctuations that are large enough to prevent detection and measurement of f_0.

To address this problem and enable $f-2f$ self-referencing of our comb, we pass the comb through a Fabry-Perot filter cavity whose free-spectral range is actively stabilized to the comb's mode spacing. The filter cavity's Lorentzian transfer function reduces the optical frequency fluctuations of the comb modes at high frequency—these fluctuations are averaged over the photon lifetime of the cavity. This enables generation of a supercontinuum with resolvable modes that is suitable for $f-2f$ self-referencing and measurement of f_0.

The filter cavity used for this 10 GHz comb has a 7.5 MHz linewidth; equivalently, it has finesse of $\mathcal{F}$ ∼1333. The effect of passing the comb through the cavity is demonstrated concretely in Fig. 1.4b, where we compare the lineshape of a heterodyne beat between the supercontinuum and a CW laser with 1319 nm wavelength with and without the filter cavity in place. The signal-to-noise ratios for the beat with and without the filter cavity are 40 dB and 17 dB, respectively.

We also explore the effect of low-frequency fluctuations in the modulation tone f_{rep} by changing the source of this tone. The f_0 signal shown in Fig. 1.3b is acquired with a tunable commercial synthesizer providing f_{rep}. In Fig. 1.5 we show the detected f_0 signal with a dielectric-resonator oscillator and a sapphire oscillator providing f_{rep}; these sources have less low-frequency noise, and the effect of this lower noise is readily apparent in the reduced linewidth of the f_0 signal. This indicates the importance of a high-performance microwave oscillator for future deployments of EOM combs.

1.4 Outlook

The EOM comb approach for frequency-comb generation yields combs that are widely tunable and that can be flexibly tailored for specific applications. Because the comb generation is a non-resonant process (up to the optional inclusion of a filter cavity), the comb properties can be manipulated in real time with speed and range that greatly exceeds the capabilities of mode-locked lasers (where repetition-rate adjustment requires manipulation of moving parts) and microcombs (where repetition-rate control via phase modulation as described in Chap. **??**, for example, is limited to the locking range afforded by the resonator dispersion). This has allowed, for example, the proposal and demonstration of 'PHIRE'—Parallel Heterodyne Interferometry via Rep-rate Exchange—which is, essentially, dual-comb spectroscopy [10] with a single frequency comb whose repetition-rate is periodically switched [111].

EOM combs, with their lack of moving parts, also offer robust turn-key operation to a degree

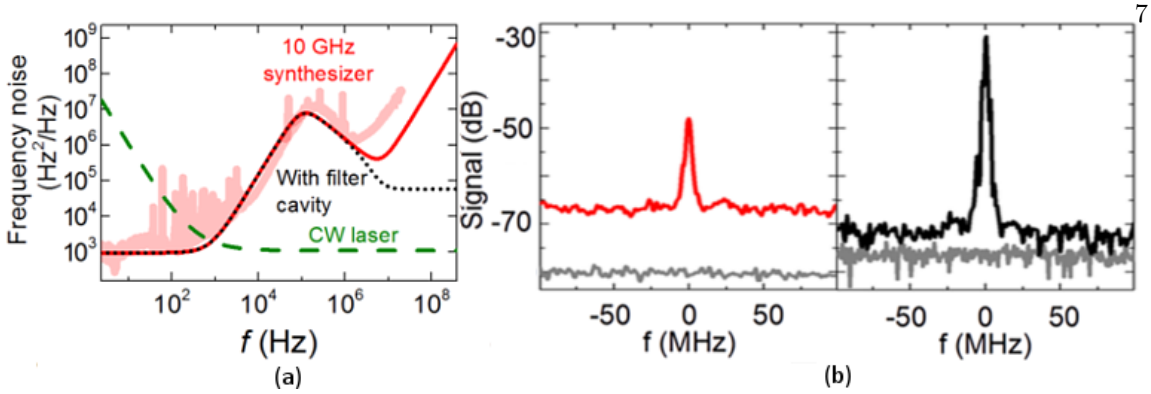

Figure 1.4: **Investigation of the noise properties of the EOM comb.** (a) Contributions to the frequency-noise spectrum of the carrier-envelope offset frequency: model of the input seed laser (dashed green), model of the 10 GHz synthesizer multipled by 19430^2 without the filter cavity (solid red, experimental data thick red), and synthesizer multiplied by 19340^2 and the Lorentzian filter-cavity transfer function (dotted black). (b) Comparison of the detected beats between the supercontinuum and a CW laser with 1319 nm wavelength without (red, left) and with (black, right) the Fabry-Perot filter cavity. The level of intensity noise on the supercontinuum, measured by removing the 1319 nm CW laser, is shown by the lower gray trace in each plot; the elevated floor of the red trace relative to this background indicates that frequency noise is responsible for the reduced SNR of the beat without the filter cavity. Signal-to-noise ratios for the beat are 17 dB without and 40 dB with the filter cavity.

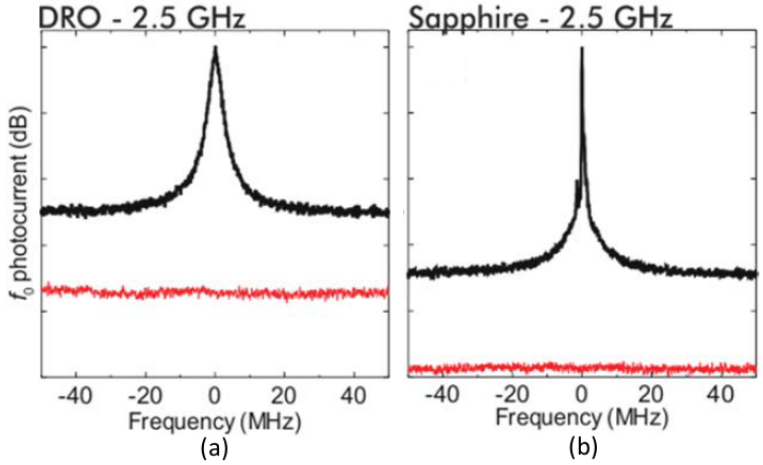

Figure 1.5: **Photodetected carrier-envelope-offset frequency signal with different sources for f_{rep}.** (a) The f_0 beat resulting from a dieletric-resonator oscillator source for the modulation frequency. (b) Ibid with a sapphire oscillator as the source for f_{rep}, which has lower noise than both the tunable commerical synthesizer and the DRO. The reduction in linewidth associated with the change in the source for f_{rep} shows the effect of low-Fourier-frequency noise of f_{rep} on the frequency-noise characteristics of the EOM comb.

that is difficult to achieve with other comb sources. This has made them particularly promising for applications where long-term deployment with maximum up-time is important, such as calibration of astronomical spectrograms [112]. While the necessity of the filter cavity described here to enable

$f - 2f$ self-referencing is an apparent limitation, there are promising routes towards eliminating this requirement—using a high-power, tunable microwave oscillator could allow self-referencing of a repetition-rate-tunable EOM comb without a filter cavity.

Appendix A

Numerical simulations of nonlinear optics

This appendix describes the algorithm used for numerical simulation of the generalized nonlinear Schrodinger equation (GNLSE) and Lugiato-Lefever equation (LLE) to obtain the results presented in the preceding chapters in this thesis. These equations are simulated with Matlab using a fourth-order Runge-Kutta interaction picture (RK4IP) method [124] with adaptive step size [123]. The RK4IP method is a particular algorithm in the broader class of split-step Fourier algorithms in which nonlinearity is implemented in the time domain and dispersion is implemented in the frequency domain. An illustrative example of the split-step Fourier approach is a far simpler algorithm carried out with a single line of Matlab code to simulate the LLE:

```
psi=ifft(exp(delta*L).*fft(exp(delta*(1i*abs(psi).^2+F./psi)).*psi));
```

where `delta` is the step size and `L` is a linear frequency-domain dispersion operator ($\hat{L}$, see below) that has been defined in the preceding code. The RK4IP algorithm with adaptive step size is advantageous over this simple algorithm in calculation time and in the scaling of error with the step size.

A.1 RK4IP algorithm

The LLE (NLSE) describes the evolution of the field ψ (A), a function of a fast variable θ (T), over a timescale parametrized by a slow variable τ (z). In what immediately follows we use the variable names corresponding to the LLE for simplicity. Each of these equations can be written as the sum of a nonlinear operator $\hat{N}$ and a linear operator $\hat{L}$ acting on ψ, so that the field ψ evolves as

$$\frac{\partial \psi}{\partial \tau} = (\hat{N} + \hat{L})\psi, \tag{A.1}$$

which can be implemented with the split-step Fourier approach.

The RK4IP algorithm specifies a recipe for advancing the field a single step δ in the slow variable τ to obtain $\psi(\theta, \tau + \delta)$ from $\psi(\theta, \tau)$. This specific algorithm has the attractive feature that it reduces the number of Fourier transformations that must be performed to achieve a given

calculation accuracy relative to other common algorithms. The RK4IP algorithm is[124]:

$$\psi_I = \exp\left(\frac{\delta}{2}\hat{L}\right)\psi(\theta,\tau) \tag{A.2}$$

$$k_1 = \exp\left(\frac{\delta}{2}\hat{L}\right)\left[\delta\tau\hat{N}(\psi(\theta,\tau))\right]\psi(\theta,\tau) \tag{A.3}$$

$$k_2 = \delta\hat{N}(\psi_I + k_1/2)\left[\psi_I + k_1/2\right] \tag{A.4}$$

$$k_3 = \delta\hat{N}(\psi_I + k_2/2)\left[\psi_I + k_2/2\right] \tag{A.5}$$

$$k_4 = \delta\hat{N}\left(\exp\left(\frac{\delta}{2}\hat{L}\right)(\psi_I + k_3)\right) \tag{A.6}$$

$$\times \exp\left(\frac{\delta}{2}\hat{L}\right)(\psi_I + k_3) \tag{A.7}$$

$$\psi(\theta,\tau+\delta) = \exp\left(\frac{\delta}{2}\hat{L}\right)\left[\psi_I + k_1/6 + k_2/3 + k_3/3\right] + k_4/6. \tag{A.8}$$

In the above it is understood that $\hat{L}$ is applied in the frequency domain and $\hat{N}$ is applied in the time domain. Calculation of $\psi(\theta,\tau+\delta)$ from $\psi(\theta,\tau)$ therefore requires eight Fourier transformations.

A.2 Adaptive step-size algorithm

An adaptive step-size algorithm is a strategy for adjusting the magnitude of the steps δ that are taken to optimize the simulation speed while maintaining a desired degree of accuracy. The RK4IP algorithm exhibits error that scales locally as $O(\delta^5)$. Since reducing the step size naturally requires more steps and therefore increases the number of small errors that accumulate, the resulting global accuracy of the algorithm is $O(\delta^4)$. One appropriate step-size adjustment algorithm for this scaling is described by Heidt [123]. For a given goal error e_G, the algorithm goes as follows:

- Calculate a field ψ_{coarse} by advancing the field $\psi(\theta,\tau)$ according to RK4IP by a step of size δ.
- Calculate a field ψ_{fine} by advancing the field $\psi(\theta,\tau)$ according to RK4IP by two steps of size $\delta/2$.
- Calculate the measured error $e = \sqrt{\sum_j |\psi_{coarse,j} - \psi_{fine,j}|^2 / \sum_j |\psi_{fine,j}|^2}$, where j indexes over the discrete points parametrizing the fast variable θ.
  - If $e > 2e_G$, discard the solution and repeat the process with coarse step size $\delta' = \delta/2$.
  - If $e_G < e < 2e_G$, the evolution continues and the step size is reduced to $\delta' = \delta/2^{1/5} \approx 0.87\delta$.
  - If $e_G/2 < e < e_G$, the evolution continues and the step size is not changed.
  - If $e < e_G/2$, the evolution continues and the step size is increased to $\delta' = 2^{1/5}\delta \approx 1.15\delta$.

When the simulation continues, the new field $\psi(\theta,\tau+\delta)$ is taken to be $\psi(\theta,\tau+\delta) = 16\psi_{fine}/15 - \psi_{coarse}/15$. In the calculations described in this thesis, the goal error e_G is typically 10^{-6}.

A.3 Pseudocode for numerical simulation with the RK4IP algorithm and adaptive step size

The pseudocode shown in Algorithm 1 shows how the RK4IP algorithm with adaptive step size is implemented. This pseudocode neglects the specific details of the RK4IP algorithm.

Two notes:

- The current field $\psi(\theta, \tau)$ is stored until the approximation to the new field $\psi(\theta, \tau + \delta)$ is found to be acceptable.
- This implementation makes use of an extra efficiency that is possible when the solution is discarded and the step size is halved: the first step of the fine solution $\psi_{fine,1}$ for the previous attempt becomes the coarse solution ψ_{coarse} for the current attempt.

Algorithm 1 Pseudocode showing the implementation of RK4IP with adaptive step size.

```
procedure
    while τ < τ_end do
        e = 1                                   ▷ Initialize the error to a large value
        firsttry = TRUE                         ▷ For more efficiency if this is not the first attempt (see below)
        δ = 2δ                                  ▷ To account for halving on the first iteration

        while e > 2e_G do
            if firsttry then
                ψ_coarse = RK4IP(ψ, δ)
            else
                ψ_coarse = ψ_fine,1             ▷ We get to re-use the first step of the previous attempt's fine solution

            δ = δ/2
            ψ_fine = ψ

            for j_step = 1 : 2 do
                ψ_fine = RK4IP(ψ_fine, δ)
                if j_step = 1 then
                    ψ_fine,1 = ψ_fine

            e = sqrt(Σ|ψ_coarse − ψ_fine|^2 / Σ|ψ_fine|^2)
            firsttry = FALSE

        ψ = 16ψ_fine/15 − ψ_coarse/15
        τ = τ + 2δ                              ▷ We took two fine steps of size δ

        if e > e_G then
            δ = δ/2^(1/5)
        if e < e_G/2 then
            δ = 2^(1/5)δ
```

A.3.1 Simulation of the LLE

For simulation of the LLE, the operators are:

$$\hat{N} = i|\psi|^2 + F/\psi, \tag{A.9}$$

$$\hat{L} = -(1 + i\alpha_\mu), \text{where} \tag{A.10}$$

$$\alpha_\mu = \alpha - \sum_{n=1}^{N} \beta_n \mu^n / n!. \tag{A.11}$$

The subscript μ indicates the pump-referenced mode number upon which the operator acts. Note, in particular, that the pump term F has been incorporated into the nonlinear operator, so that it is implemented in the time domain. The quantity $\hat{N}\psi$ then becomes $i|\psi|^2\psi + F$, as required for computation of $\partial\psi/\partial\tau$.

A.3.2 Simulation of the GNLSE

The GNLSE used in the simulations conducted for Chapter **??** contains nonlinear terms that describe the medium's Raman response and self-steepening. The equation employed can be written

as [27, 124]:

$$\frac{\partial A}{\partial z} = -\left(\sum_n \beta_n \frac{i^{n-1}}{n!}\frac{\partial^n}{\partial T^n}\right) A + i\gamma\left(1+\frac{1}{\omega_0}\frac{\partial}{\partial T}\right) \times \left((1-f_R)A|A|^2 + f_R A\int_0^\infty h_R(\tau)|A(z,T-\tau)|^2 d\tau\right). \quad \text{(A.12)}$$

For Chapter **??**, second- and third-order dispersion is used with β_2 =-7.7 ps^2/km and β_3 =0.055 ps^3/km, where β_n is the n^{th} frequency-derivative of the propagation constant. The nonlinear coefficient $\gamma = \frac{2\pi}{\lambda}\frac{n_2}{A_{eff}}$ used is 11 W/km [118], coming from an effective mode-field diameter of $\sim$3.5 μm for the HNLF used in the experiment and the nonlinear index $n_2 = 2.7\times10^{-16}$ cm^2/W of silica. The quantity $\omega_0 = 2\pi c/\lambda_0$ is the (angular) carrier frequency of the pulse, and the parameter $f_R = 0.18$ and function

$$h_R(\tau > 0) = (\tau_1^2+\tau_2^2)/(\tau_1\tau_2^2)\times e^{-\tau/\tau_2}\sin\tau/\tau_1 \quad \text{(A.13)}$$

describe the medium's Raman response, with $\tau_1 = 12.2$ fs and $\tau_2 = 32$ fs used here [27, 124, 127].

The linear frequency-domain operator applied in the RK4IP algorithm is

$$\hat{L} = i\frac{\beta_2}{2}(\omega_\mu-\omega_0)^2 - \frac{\beta_3}{6}(\omega_\mu-\omega_0)^3 \quad \text{(A.14)}$$

Here ω_μ is defined by the discretization of the frequency domain due to Fourier-transformation of a finite temporal window of length T_{comp} via $\omega_\mu = \omega_0 + 2\pi\mu/T_{comp}$; where T_{comp} is the size of the domain for the fast time variable T.

The nonlinear operator $\hat{N}$ for the GNLSE implements the convolution as a product in the frequency domain. That is,

$$\hat{N} = i\gamma\frac{1}{A}\left(1+\frac{1}{\omega_0}\frac{\partial}{\partial T}\right)\times\left[(1-f_R)A|A|^2 + f_R A\,\mathcal{F}^{-1}\left\{\chi_R\cdot\mathcal{F}(|A|^2)\right\}\right], \quad \text{(A.15)}$$

where $\chi_R = \mathcal{F}\{h_R(\tau)\}$ and $\mathcal{F}$ denotes Fourier transformation. Procedurally, the quantity in the square brackets is calculated first, and then the fast-time derivative is implemented and the sum in the curved brackets is calculated.

References

[1] S. A. Diddams, D. J. Jones, J. Ye, S. T. Cundiff, J. L. Hall, J. K. Ranka, R. S. Windeler, R. Holzwarth, T. Udem, and T. W. Hänsch. Direct link between microwave and optical frequencies with a 300 THz femtosecond laser comb. *Physical Review Letters*, 84 (22), **2000**, 5102–5105. DOI: 10.1103/PhysRevLett.84.5102.

[2] D. J. Jones, S. A. Diddams, J. K. Ranka, A. Stentz, R. S. Windeler, J. L. Hall, and S. T. Cundiff. Carrier-Envelope Phase Control of Femtosecond Mode-Locked Lasers and Direct Optical Frequency Synthesis. *Science*, 288 (5466), **2000**, 635–639.

[3] T. Udem, R Holzwarth, and T. W. Hänsch. Optical frequency metrology. *Nature*, 416 (6877), **2002**, 233–237. DOI: 10.1038/416233a.

[4] J. L. Hall. Nobel lecture: Defining and measuring optical frequencies. *Reviews of Modern Physics*, 78 (4), **2006**, 1279–1295. DOI: 10.1103/RevModPhys.78.1279.

[5] T. W. Hänsch. Nobel lecture: Passion for precision. *Reviews of Modern Physics*, 78 (4), **2006**, 1297–1309. DOI: 10.1103/RevModPhys.78.1297.

[6] J. K. Ranka, R. S. Windeler, and A. J. Stentz. Visible continuum generation in air–silica microstructure optical fibers with anomalous dispersion at 800 nm. *Optics Letters*, 25 (1), **2000**, 25. DOI: 10.1364/OL.25.000025.

[7] S. A. Diddams, T. Udem, J. C. Bergquist, E. A. Curtis, R. E. Drullinger, L Hollberg, W. M. Itano, W. D. Lee, C. W. Oates, K. R. Vogel, and D. J. Wineland. An Optical Clock Based on a Single Trapped 199 Hg+ Ion. *Science (New York, N.Y.)*, 293, **2001**, 825–828. DOI: 10.1126/science.1061171.

[8] T. M. Fortier, M. S. Kirchner, F. Quinlan, J. Taylor, J. C. Bergquist, T. Rosenband, N. Lemke, A. Ludlow, Y. Jiang, C. W. Oates, and S. A. Diddams. Generation of ultrastable microwaves via optical frequency division. *Nature Photonics*, 5 (7), **2011**, 425–429. DOI: 10.1038/nphoton.2011.121. arXiv: 1101.3616.

[9] S. A. Diddams, L. Hollberg, and V. Mbele. Molecular fingerprinting with the resolved modes of a femtosecond laser frequency comb. *Nature*, 445 (7128), **2007**, 627–630. DOI: 10.1038/nature05524.

[10] I. Coddington, N. Newbury, and W. Swann. Dual-comb spectroscopy. *Optica*, 3 (4), **2016**, 414–426. DOI: 10.1364/OPTICA.3.000414 (cited on page 6).

[11] S. T. Cundiff and A. M. Weiner. Optical arbitrary waveform generation. *Nature Photonics*, 4 (11), **2010**, 760–766. DOI: 10.1038/nphoton.2010.196.

[12] T. Steinmetz, T. Wilken, C. Araujo-Hauck, R. Holzwarth, T. W. Hänsch, L. Pasquini, A. Manescau, S. D'Odorico, M. T. Murphy, T. Kentischer, W. Schmidt, and T. Udem. Laser frequency combs for astronomical observations. *Science*, 321 (5894), **2008**, 1335–7. DOI: 10.1126/science.1161030.

[13] B. R. Washburn, S. A. Diddams, N. R. Newbury, J. W. Nicholson, M. F. Yan, and C. G. Jørgensen. Phase-locked, erbium-fiber-laser-based frequency comb in the near infrared. *Optics Letters*, 29 (3), **2004**, 250–252. DOI: 10.1364/OL.29.000250.

[14] C. Gohle, T. Udem, M. Herrmann, J. Rauschenberger, R. Holzwarth, H. A. Schuessler, F. Krausz, and T. W. Hänsen. A frequency comb in the extreme ultraviolet. *Nature*, 436 (7048), **2005**, 234–237. DOI: 10.1038/nature03851.

[15] S. A. Diddams. The evolving optical frequency comb [Invited]. *Journal of the Optical Society of America B*, 27 (11), **2010**, B51–B62. DOI: 10.1364/JOSAB.27.000B51.

[16] J. Faist, G. Villares, G. Scalari, M. Rosch, C. Bonzon, A. Hugi, and M. Beck. Quantum Cascade Laser Frequency Combs. *Nanophotonics*, 5 (2), **2016**, 272–291. DOI: 10.1515/nanoph-2016-0015. arXiv: 1510.09075.

[17] D. T. Spencer, T. Drake, T. C. Briles, J. Stone, L. C. Sinclair, C. Fredrick, Q. Li, D. Westly, B. R. Ilic, A. Bluestone, N. Volet, T. Komljenovic, L. Chang, S. H. Lee, D. Y. Oh, T. J. Kippenberg, E. Norberg, L. Theogarajan, M.-g. Suh, K. Y. Yang, H. P. Martin, K. Vahala, N. R. Newbury, K. Srinivasan, J. E. Bowers, S. A. Diddams, and S. B. Papp. An optical-frequency synthesizer using integrated photonics. *Nature*, 557, **2018**, 81–85. DOI: 10.1038/s41586-018-0065-7.

[18] R. W. Boyd. **Nonlinear Optics**. San Diego, CA: Elsevier, 2003.

[19] T. M. Fortier, D. J. Jones, and S. T. Cundiff. Phase stabilization of an octave-spanning Ti:sapphire laser. *Opt. Lett.*, 28 (22), **2003**, 2198–2200. DOI: 10.1364/OL.28.002198.

[20] T. J. Kippenberg, R Holzwarth, and S. A. Diddams. Microresonator-Based Optical Frequency Combs. *Science (New York, N.Y.)*, 332 (6029), **2011**, 555–559. DOI: 10.1126/science.1193968.

[21] A. A. Savchenkov, A. B. Matsko, and L Maleki. On Frequency Combs in Monolithic Resonators. *Nanophotonics*, 5, **2016**, 363–391. DOI: 10.1515/nanoph-2016-0031.

[22] Y. K. Chembo. Kerr optical frequency combs: Theory, applications and perspectives. *Nanophotonics*, 5 (2), **2016**, 214–230. DOI: 10.1515/nanoph-2016-0013.

[23] A. Pasquazi, M. Peccianti, L. Razzari, D. J. Moss, S. Coen, M. Erkintalo, Y. K. Chembo, T. Hansson, S. Wabnitz, P. Del'Haye, X. Xue, A. M. Weiner, and R. Morandotti. Micro-combs: A novel generation of optical sources. *Physics Reports*, 729, **2017**, 1–81. DOI: 10.1016/j.physrep.2017.08.004.

[24] E. Obrzud, S. Lecomte, and T. Herr. Temporal solitons in microresonators driven by optical pulses. *Nature Photonics*, 11 (August), **2017**, 600–607. DOI: 10.1038/nphoton.2017.140. arXiv: 1612.08993.

[25] H. Lee, T. Chen, J. Li, K. Y. Yang, S. Jeon, O. Painter, and K. J. Vahala. Chemically etched ultrahigh-Q wedge-resonator on a silicon chip. *Nature Photonics*, 6 (6), **2012**, 369–373. DOI: 10.1038/nphoton.2012.109. arXiv: 1112.2196.

[26] K. Y. Yang, K. Beha, D. C. Cole, X. Yi, P. Del'Haye, H. Lee, J. Li, D. Y. Oh, S. A. Diddams, S. B. Papp, and K. J. Vahala. Broadband dispersion-engineered microresonator on a chip. *Nature Photonics*, 10 (March), **2016**, 316–320. DOI: 10.1038/nphoton.2016.36.

[27] G. P. Agrawal. **Nonlinear Fiber Optics**. 4th. Burlington, MA: Elsevier, 2007 (cited on pages 3, 12).

[28] M. L. Calvo and V. Lakshminarayanan, eds. **Optical Waveguides: From Theory to Applied Technologies**. Boca Raton, FL: Taylor & Francis, 2007.

[29] P. Del'Haye, S. A. Diddams, and S. B. Papp. Laser-machined ultra-high-Q microrod resonators for nonlinear optics. *Applied Physics Letters*, 102, **2013**, 221119.

[30] A. N. Oraevsky. Whispering-gallery waves. *Quantum Electronics*, 32 (42), **2002**, 377–400. DOI: 10.1070/QE2001v031n05ABEH002205. arXiv: arXiv:1011.1669v3.

[31] H. A. Haus. **Waves and Fields in Optoelectronics**. Englewood Cliffs: Prentice-Hall, 1984.

[32] S. M. Spillane, T. J. Kippenberg, O. J. Painter, and K. J. Vahala. Ideality in a Fiber-Taper-Coupled Microresonator System for Application to Cavity Quantum Electrodynamics. *Physical review letters*, 91 (4), **2003**, 043902. DOI: 10.1103/PhysRevLett.91.043902.

[33] V. S. Il'chenko and M. L. Gorodetskii. Thermal nonlinear effects in optical whispering gallery microresonators.pdf. *Laser Physics*, 2 (6), **1992**, 1004–1009.

[34] T. Carmon, L. Yang, and K. J. Vahala. Dynamical thermal behavior and thermal self-stability of microcavities. *Optics Express*, 12 (20), **2004**, 4742–4750. URL: http://www.ncbi.nlm.nih.gov/pubmed/19484026http://www.opticsinfobase.org/oe/abstract.cfm?uri=oe-12-20-4742.

[35] R. del Coso and J. Solis. Relation between nonlinear refractive index and third-order susceptibility in absorbing media. *Journal of the Optical Society of America B*, 21 (3), **2004**, 640. DOI: 10.1364/JOSAB.21.000640.

[36] P Del'Haye, A Schliesser, O Arcizet, T Wilken, R Holzwarth, and T. J. Kippenberg. Optical frequency comb generation from a monolithic microresonator. *Nature*, 450 (7173), **2007**, 1214–1217. DOI: 10.1038/nature06401.

[37] T. Kippenberg, S. Spillane, and K. Vahala. Kerr-Nonlinearity Optical Parametric Oscillation in an Ultrahigh-Q Toroid Microcavity. *Physical Review Letters*, 93 (8), **2004**, 083904. DOI: 10.1103/PhysRevLett.93.083904.

[38] A. A. Savchenkov, A. B. Matsko, D. Strekalov, M. Mohageg, V. S. Ilchenko, and L. Maleki. Low threshold optical oscillations in a whispering gallery mode CaF 2 resonator. *Physical Review Letters*, 93 (24), **2004**, 2–5. DOI: 10.1103/PhysRevLett.93.243905.

[39] I. H. Agha, Y. Okawachi, M. A. Foster, J. E. Sharping, and A. L. Gaeta. Four-wave-mixing parametric oscillations in dispersion-compensated high- Q silica microspheres. *Physical Review A - Atomic, Molecular, and Optical Physics*, 76 (4), **2007**, 1–4. DOI: 10.1103/PhysRevA.76.043837.

[40] T. Herr, V. Brasch, J. D. Jost, C. Y. Wang, N. M. Kondratiev, M. L. Gorodetsky, and T. J. Kippenberg. Temporal solitons in optical microresonators. *arXiv*, **2012**, 1211.0733. DOI: 10.1038/nphoton.2013.343. arXiv: 1211.0733.

[41] T. Herr, V. Brasch, J. D. Jost, C. Y. Wang, N. M. Kondratiev, M. L. Gorodetsky, and T. J. Kippenberg. Temporal solitons in optical microresonators. *Nature Photonics*, 8 (2), **2014**, 145–152. DOI: 10.1109/CLEOE-IQEC.2013.6801769. arXiv: 1211.0733.

[42] F. Leo, S. Coen, P. Kockaert, S.-P. Gorza, P. Emplit, and M. Haelterman. Temporal cavity solitons in one-dimensional Kerr media as bits in an all-optical buffer. *Nature Photonics*, 4 (7), **2010**, 471–476. DOI: 10.1038/nphoton.2010.120.

[43] T. Herr, K. Hartinger, J. Riemensberger, C. Y. Wang, E. Gavartin, R. Holzwarth, M. L. Gorodetsky, and T. J. Kippenberg. Universal formation dynamics and noise of Kerr-frequency combs in microresonators. *Nature Photonics*, 6 (7), **2012**, 480–487. DOI: 10.1038/nphoton.2012.127.

[44] Y. K. Chembo and C. R. Menyuk. Spatiotemporal Lugiato-Lefever formalism for Kerr-comb generation in whispering-gallery-mode resonators. *Physical Review A*, 87, **2013**, 053852. DOI: 10.1103/PhysRevA.87.053852.

[45] S. Coen, H. G. Randle, T. Sylvestre, and M. Erkintalo. Modeling of octave-spanning Kerr frequency combs using a generalized mean-field Lugiato-Lefever model. *Optics letters*, 38 (1), **2013**, 37–39. URL: http://www.ncbi.nlm.nih.gov/pubmed/23282830.

[46] M. Haelterman, S. Trillo, and S. Wabnitz. Dissipative modulation instability in a nonlinear dispersive ring cavity. *Optics Communications*, 91 (5-6), **1992**, 401–407. DOI: 10.1016/0030-4018(92)90367-Z.

[47] T Hansson, M Bernard, and S Wabnitz. Modulational Instability of Nonlinear Polarization Mode Coupling in Microresonators. 35 (4), **2018**. URL: https://arxiv.org/pdf/1802.04535.pdf. arXiv: arXiv:1802.04535v1.

[48] Y. K. Chembo, I. S. Grudinin, and N Yu. Spatiotemporal dynamics of Kerr-Raman optical frequency combs. *Physical Review A*, 92 (4), **2015**, 4. DOI: 10.1103/PhysRevA.92.043818.

[49] C. Godey, I. V. Balakireva, A. Coillet, and Y. K. Chembo. Stability analysis of the spatiotemporal Lugiato-Lefever model for Kerr optical frequency combs in the anomalous and normal dispersion regimes. *Physical Review A*, 89 (6), **2014**, 063814. DOI: 10.1103/PhysRevA.89.063814.

[50] I. V. Barashenkov and Y. S. Smirnov. Existence and stability chart for the ac-driven, damped nonlinear Schrödinger solitons. *Physical Review E - Statistical Physics, Plasmas, Fluids, and Related Interdisciplinary Topics*, 54 (5), **1996**, 5707–5725. DOI: 10.1103/PhysRevE.54.5707.

[51] A Coillet and Y. K. Chembo. Routes to spatiotemporal chaos in Kerr optical frequency combs. *Chaos*, 24 (1), **2014**, 5. DOI: 10.1063/1.4863298. arXiv: arXiv:1401.0927v1.

[52] L. A. Lugiato and R Lefever. Spatial Dissipative Structures in Passive Optical Systems. *Physical Review Letters*, 58 (21), **1987**, 2209–2211.

[53] L. Lugiato and R Lefever. Diffraction stationary patterns in passive optical systems. *Interaction of Radiation with Matter*, **1987**.

[54] W. H. Renninger and P. T. Rakich. Closed-form solutions and scaling laws for Kerr frequency combs. *Scientific Reports*, 6 (1), **2016**, 24742. DOI: 10.1038/srep24742. arXiv: 1412.4164.

[55] S. Coen and M. Erkintalo. Universal scaling laws of Kerr frequency combs. *Optics letters*, 38 (11), **2013**, 1790–1792. DOI: 10.1364/OL.38.001790. arXiv: arXiv:1303.7078v1.

[56] Y. Wang, F. Leo, J. Fatome, M. Erkintalo, S. G. Murdoch, and S. Coen. Universal mechanism for the binding of temporal cavity solitons, **2017**, 1–10. URL: http://arxiv.org/abs/1703.10604. arXiv: 1703.10604.

[57] P. Parra-Rivas, D. Gomila, P. Colet, and L. Gelens. Interaction of solitons and the formation of bound states in the generalized Lugiato-Lefever equation. *European Physical Journal D*, 71 (7), **2017**, 198. DOI: 10.1140/epjd/e2017-80127-5. arXiv: arXiv:1705.02619v1.

[58] V. Brasch, T. Herr, M. Geiselmann, G. Lihachev, M. H. P. Pfeiffer, M. L. Gorodetsky, and T. J. Kippenberg. Photonic chip-based optical frequency comb using soliton Cherenkov radiation. *Science*, 351 (6271), **2016**, 357. DOI: 10.1364/CLEO_SI.2015.STh4N.1. arXiv: 1410.8598.

[59] X. Yi, Q.-F. Yang, K. Y. Yang, M.-G. Suh, and K. Vahala. Soliton frequency comb at microwave rates in a high-Q silica microresonator. *Optica*, 2 (12), **2015**, 1078–1085.

[60] V. E. Lobanov, G. V. Lihachev, N. G. Pavlov, A. V. Cherenkov, T. J. Kippenberg, and M. L. Gorodetsky. Harmonization of chaos into a soliton in Kerr frequency combs. *Optics Express*, 24 (24), **2016**, 27382. DOI: 10.1126/science.aah4243. arXiv: 1607.08222.

[61] C. Joshi, J. K. Jang, K. Luke, X. Ji, S. A. Miller, A. Klenner, Y. Okawachi, M. Lipson, and A. L. Gaeta. Thermally controlled comb generation and soliton modelocking in microresonators. *Optics Letters*, 41 (11), **2016**, 2565–2568. DOI: 10.1364/OL.41.002565. arXiv: 1603.08017.

[62] W. Wang, Z. Lu, W. Zhang, S. T. Chu, B. E. Little, L. Wang, X. Xie, M. Liu, Q. Yang, L. Wang, J. Zhao, G. Wang, Q. Sun, Y. Liu, Y. Wang, and W. Zhao. Robust soliton crystals in a thermally controlled microresonator. *Optics Letters*, 43 (9), **2018**, 2002–2005. DOI: 10.1364/OL.43.002002.

[63] H. Guo, M. Karpov, E. Lucas, A. Kordts, M. H. Pfeiffer, V. Brasch, G. Lihachev, V. E. Lobanov, M. L. Gorodetsky, and T. J. Kippenberg. Universal dynamics and deterministic switching of dissipative Kerr solitons in optical microresonators. *Nature Physics*, 13 (1), **2017**, 94–102. DOI: 10.1038/nphys3893. arXiv: 1601.05036.

[64] J. K. Jang, M. Erkintalo, S. G. Murdoch, and S. Coen. Writing and erasing of temporal cavity solitons by direct phase modulation of the cavity driving field. *Optics Letters*, 40 (20), **2015**, 4755–4758. DOI: 10.1364/OL.40.004755. arXiv: 1501.05289.

[65] J. K. Jang, M. Erkintalo, S. Coen, and S. G. Murdoch. Temporal tweezing of light through the trapping and manipulation of temporal cavity solitons. *Nature Communications*, 6, **2015**, 7370. DOI: 10.1038/ncomms8370. arXiv: 1410.4836.

[66] Y. Wang, B. Garbin, F. Leo, S. Coen, M. Erkintalo, and S. G. Murdoch. Writing and Erasure of Temporal Cavity Solitons via Intensity Modulation of the Cavity Driving Field. *arXiv*, **2018**, 1802.07428. arXiv: 1802.07428.

[67] S. B. Papp, K. Beha, P. Del'Haye, F. Quinlan, H. Lee, K. J. Vahala, and S. A. Diddams. Microresonator frequency comb optical clock. *Optica*, 1 (1), **2014**, 10–14. DOI: 10.1364/OPTICA.1.000010. arXiv: 1309.3525.

[68] M. G. Suh, Q. F. Yang, K. Y. Yang, X. Yi, and K. J. Vahala. Microresonator soliton dual-comb spectroscopy. *Science*, 354 (6312), **2016**, 1–5. DOI: 10.1126/science.aah6516. arXiv: 1607.08222.

[69] P. Marin-Palomo, J. N. Kemal, M. Karpov, A. Kordts, J. Pfeifle, M. H. Pfeiffer, P. Trocha, S. Wolf, V. Brasch, M. H. Anderson, R. Rosenberger, K. Vijayan, W. Freude, T. J. Kippenberg, and C. Koos. Microresonator-based solitons for massively parallel coherent optical communications. *Nature*, 546 (7657), **2017**, 274–279. DOI: 10.1038/nature22387. arXiv: 1610.01484.

[70] J. D. Jost, T. Herr, C. Lecaplain, V. Brasch, M. H. P. Pfeiffer, and T. J. Kippenberg. Counting the cycles of light using a self-referenced optical microresonator. *Optica*, 2 (8), **2015**, 706–711. DOI: 10.1364/OPTICA.2.000706. arXiv: 1411.1354.

[71] P. Del'Haye, A. Coillet, T. Fortier, K. Beha, D. C. Cole, K. Y. Yang, H. Lee, K. J. Vahala, S. B. Papp, and S. A. Diddams. Phase-coherent microwave-to-optical link with a self-referenced microcomb. *Nature Photonics*, 10 (June), **2016**, 1–5. DOI: 10.1038/nphoton.2016.105.

[72] V. Brasch, E. Lucas, J. D. Jost, M. Geiselmann, and T. J. Kippenberg. Self-referenced photonic chip soliton Kerr frequency comb. *Light: Science & Applications*, 6 (1), **2017**, e16202. DOI: 10.1038/lsa.2016.202. arXiv: 1605.02801.

[73] T. C. Briles, J. R. Stone, T. E. Drake, D. T. Spencer, C. Frederick, Q. Li, D. A. Westly, B. R. Illic, K. Srinivasan, S. A. Diddams, and S. B. Papp. Kerr-microresonator solitons for accurate carrier-envelope-frequency stabilization. *arXiv*, **2017**, 1711.06251. URL: http://arxiv.org/abs/1711.06251. arXiv: 1711.06251.

[74] H. Taheri, A. A. Eftekhar, K. Wiesenfeld, and A. Adibi. Soliton formation in whispering-gallery-mode resonators via input phase modulation. *IEEE Photonics Journal*, 7 (2), **2015**, 2200309. DOI: 10.1109/JPHOT.2015.2416121.

[75] J. R. Stone, T. C. Briles, T. E. Drake, D. T. Spencer, D. R. Carlson, S. A. Diddams, and S. B. Papp. Thermal and Nonlinear Dissipative-Soliton Dynamics in Kerr Microresonator Frequency Combs. *arXiv*, **2017**, 1708.08405. URL: http://arxiv.org/abs/1708.08405. arXiv: 1708.08405.

[76] M. Zajnulina, M. Böhm, D. Bodenmüller, K. Blow, J. C. Boggio, A. Rieznik, and M. Roth. Characteristics and stability of soliton crystals in optical fibres for the purpose of optical frequency comb generation. *Optics Communications*, 393 (November 2016), **2017**, 95–102. DOI: 10.1016/j.optcom.2017.02.035.

[77] A. Haboucha, H. Leblond, M. Salhi, A. Komarov, and F. Sanchez. Coherent soliton pattern formation in a fiber laser. *Optics Letters*, 33 (5), **2008**, 524–526. DOI: 10.1364/OL.33.000524.

[78] F. Amrani, M. Salhi, P. Grelu, H. Leblond, and F. Sanchez. Universal soliton pattern formations in passively mode-locked fiber lasers. *Optics letters*, 36 (9), **2011**, 1545–1547. DOI: 10.1364/OL.36.001545.

[79] A. Haboucha, H. Leblond, M. Salhi, A. Komarov, and F. Sanchez. Analysis of soliton pattern formation in passively mode-locked fiber lasers. *Physical Review A*, 78, **2008**, 043806. DOI: 10.1103/PhysRevA.78.043806.

[80] B. A. Malomed, A Schwache, and F Mitschke. Soliton lattice and gas in passive fiber-ring resonators. *Fiber and Integrated Optics*, 17 (4), **1998**, 267–277. DOI: 10.1080/014680398244867.

[81] F. Mitschke and A. Schwache. Soliton ensembles in a nonlinear resonator. *Journal of Optics B: Quantum and Semiclassical Optics*, 10 (6), **1998**, 779–788.

[82] A. Schwache and F. Mitschke. Properties of an optical soliton gas. *Physical Review E*, 55 (6), **1997**, 7720–7725. DOI: 10.1103/PhysRevE.55.7720.

[83] H. A. Haus and W. Huang. Coupled-Mode Theory. *Proceedings of the IEEE*, 79 (10), **1991**, 1505–1518. DOI: 10.1109/5.104225.

[84] A. A. Savchenkov, A. B. Matsko, W Liang, V. S. Ilchenko, D Seidel, and L Maleki. Kerr frequency comb generation in overmoded resonators. *Opt Express*, 20 (24), **2012**, 27290–27298. DOI: 10.1364/OE.20.027290\r10.1364/OE.20.027290.. arXiv: arXiv:1201.1959v1.

[85] T. Herr, V. Brasch, J. D. Jost, I. Mirgorodskiy, G. Lihachev, M. L. Gorodetsky, and T. J. Kippenberg. Mode Spectrum and Temporal Soliton Formation in Optical Microresonators. *Physical Review Letters*, 113 (12), **2014**, 123901. DOI: 10.1103/PhysRevLett.113.123901.

[86] Y. Liu, Y. Xuan, X. Xue, P.-H. Wang, S. Chen, A. J. Metcalf, J. Wang, D. E. Leaird, M. Qi, and A. M. Weiner. Investigation of mode coupling in normal-dispersion silicon nitride microresonators for Kerr frequency comb generation. *Optica*, 1 (3), **2014**, 137–144. DOI: 10.1364/OPTICA.1.000137.

[87] X. Xue, Y. Xuan, Y. Liu, P.-H. Wang, S. Chen, J. Wang, D. E. Leaird, M. Qi, and A. M. Weiner. Mode-locked dark pulse Kerr combs in normal-dispersion microresonators. *Nat Photon*, 9 (9), **2015**, 594–600. DOI: 10.1038/nphoton.2015.137.

[88] C. Bao, Y. Xuan, D. E. Leaird, S. Wabnitz, M. Qi, and A. M. Weiner. Spatial mode-interaction induced single soliton generation in microresonators. *Optica*, 4 (9), **2017**, 1011. DOI: 10.1364/OPTICA.4.001011.

[89] T. Hansson and S. Wabnitz. Bichromatically pumped microresonator frequency combs. *Physical Review A*, 90, **2014**, 013811. DOI: 10.1103/PhysRevA.90.013811. arXiv: 1404.2792.

[90] D. V. Skryabin and W. J. Firth. Interaction of cavity solitons in degenerate optical parametric oscillators. *Optics letters*, 24 (15), **1999**, 1056–1058. DOI: 10.1364/OL.24.001056. arXiv: 9906004 [patt-sol].

[91] S. Wabnitz. Control of soliton train transmission, storage, and clock recovery by cw light injection. *Journal of the Optical Society of America B*, 13 (12), **1996**, 2739–2749. URL: http://www.scopus.com/inward/record.url?eid=2-s2.0-0030378988{\&}partnerID=tZOtx3y1.

[92] J. A. Barker and D. Henderson. What is "liquid"? Understanding the states of matter. *Reviews of Modern Physics*, 48 (4), **1976**, 587–671. DOI: 10.1103/RevModPhys.48.587.

[93] T. Egami and S. Billinge. **Underneath the Bragg Peaks**. 2nd. Oxford, UK: Elsevier, 2012, p. 422.

[94] N. W. Ashcroft and D. N. Mermin. **Solid State Physics**. 1st ed. Belmont, CA: Brooks/Cole, 1976, p. 826.

[95] A. Weiner. **Ultrafast Optics**. 1st ed. Hoboken, NJ: Wiley, 2009, p. 598.

[96] T. Kobayashi, T. Sueta, Y. Cho, and Y. Matsuo. High-repetition-rate optical pulse generator using a Fabry-Perot electro-optic modulator. *Applied Physics Letters*, 21 (8), **1972**, 341–343. DOI: 10.1063/1.1654403 (cited on page 1).

[97] M. Kourogi, K. Nakagawa, and M. Ohtsu. Wide-Span Optical Frequency Comb Generator for. 29 (10), **1993** (cited on page 1).

[98] H. Murata, A. Morimoto, T. Kobayashi, and S. Yamamoto. Optical pulse generation by electrooptic-modulation method and its application to integrated ultrashort pulse generators. *IEEE Journal of Selected Topics in Quantum Electronics*, 6 (6), **2000**, 1325–1331. DOI: 10.1109/2944.902186 (cited on page 1).

[99] T. Sakamoto, T. Kawanishi, and M. Izutsu. Asymptotic formalism for ultraflat optical frequency comb generation using a Mach-Zehnder modulator. *Optics letters*, 32 (11), **2007**, 1515–1517. DOI: 10.1364/OL.32.001515 (cited on page 1).

[100] I. Morohashi, T. Sakamoto, H. Sotobayashi, T. Kawanishi, I. Hosako, and M. Tsuchiya. Widely repetition-tunable 200 fs pulse source using a Mach-Zehnder-modulator-based flat comb generator and dispersion-flattened dispersion-decreasing fiber. *Optics letters*, 33 (11), **2008**, 1192–1194. DOI: 10.1364/OL.33.001192 (cited on page 1).

[101] A. Ishizawa, T. Nishikawa, A. Mizutori, H. Takara, S. Aozasa, A. Mori, H. Nakano, A. Takada, and M. Koga. Octave-spanning frequency comb generated by 250 fs pulse train emitted from 25 GHz externally phase-modulated laser diode for carrier-envelope-offset-locking. *Electronics Letters*, 46 (19), **2010**, 1343. DOI: 10.1049/el.2010.2228 (cited on page 1).

[102] R. Wu, V. R. Supradeepa, C. M. Long, D. E. Leaird, and A. M. Weiner. Generation of very flat optical frequency combs from continuous-wave lasers using cascaded intensity and phase modulators driven by tailored radio frequency waveforms. *Optics Letters*, 35 (19), **2010**, 3234. DOI: 10.1364/OL.35.003234. arXiv: 1005.5373 (cited on page 1).

[103] V. R. Supradeepa and A. M. Weiner. Bandwidth scaling and spectral flatness enhancement of optical frequency combs from phase-modulated continuous-wave lasers using cascaded four-wave mixing. *Optics Letters*, 37 (15), **2012**, 3066. DOI: 10.1364/OL.37.003066 (cited on page 1).

[104] A. J. Metcalf, V. Torres-company, D. E. Leaird, S. Member, A. M. Weiner, and A. Broadband. High-Power Broadly Tunable Electrooptic Frequency Comb Generator. *IEEE Journal of Selected Topics in Quantum Electronics*, 19 (6), **2013**, 3500306. URL: http://ieeexplore.ieee.org/stamp/stamp.jsp?arnumber=06553388 (cited on page 1).

[105] R. Wu, V. Torres-company, D. E. Leaird, and A. M. Weiner. Optical Frequency Comb Generation. 21 (5), **2013**, 6045–6052. DOI: 10.1364/OE.21.006045 (cited on page 1).

[106] J. M. Dudley, G. G. Genty, and S. Coen. Supercontinuum generation in photonic crystal fiber. *Reviews of Modern Physics*, 78 (4), **2006**, 1135–1184. DOI: 10.1103/RevModPhys.78.1135 (cited on page 3).

[107] A. M. Weiner. Femtosecond pulse shaping using spatial light modulators. *Review of Scientific Instruments*, 71 (5), **2000**, 1929–1960. DOI: 10.1063/1.1150614 (cited on page 4).

[108] K. Beha, D. C. Cole, P. Del'Haye, A. Coillet, S. A. Diddams, and S. B. Papp. Electronic synthesis of light. *Optica*, 4 (4), **2017**, 406–411. DOI: 10.1364/OPTICA.4.000406 (cited on page 4).

[109] a. a. Amorim, M. V. Tognetti, P Oliveira, J. L. Silva, L. M. Bernardo, F. X. Kärtner, and H. M. Crespo. Sub-two-cycle pulses by soliton self-compression in highly nonlinear photonic crystal fibers. *Optics letters*, 34 (24), **2009**, 3851–3853. DOI: 10.1364/OL.34.003851 (cited on page 5).

[110] G. Di Domenico, S. Schilt, and P. Thomann. Simple approach to the relation between laser frequency noise and laser line shape. *Applied optics*, 49 (25), **2010**, 4801–4807. DOI: 10.1364/AO.49.004801 (cited on page 6).

[111] D. R. Carlson, D. D. Hickstein, D. C. Cole, S. A. Diddams, and S. B. Papp. Dual-comb interferometry via repetition-rate switching of a single frequency comb. *arXiv*, **2018**, 1806.05311. URL: http://arxiv.org/abs/1806.05311. arXiv: 1806.05311 (cited on page 6).

[112] A. J. Metcalf, C. Bender, S. Blakeslee, W. Brand, D. Carlson, S. A. Diddams, C. Fredrick, S. Halverson, F. Hearty, D. Hickstein, J. Jennings, S. Kanodia, K. Kaplan, E. Lubar, S. Mahadevan, A. Monson, J. Ninan, C. Nitroy, S. Papp, L. Ramsey, P. Robertson, A. Roy, C. Schwab, K. Srinivasan, G. K. Stefansson, and R. Terrien. Infrared Astronomical Spectroscopy for Radial Velocity Measurements with 10 cm/s Precision. In: **Conference on Lasers and Electro-Optics**. 2018, JTh5A.1 (cited on page 7).

[113] S. Backus, C. G. Durfee, M. M. Murnane, and H. C. Kapteyn. High power ultrafast lasers. *Review of Scientific Instruments*, 69 (3), **1998**, 1207. DOI: 10.1063/1.1148795.

[114] A. Baltuska, M. Uiberacker, E. Goulielmakis, R. Kienberger, V. S. Yakovlev, T. Udem, T. W. Hänsch, and F. Krausz. Phase-Controlled Amplification of Few-Cycle Laser Pulses. *IEEE Journal of Selected Topics in Quantum Electronics*, 9 (4), **2003**, 972–989.

[115] C. Gohle, J. Rauschenberger, T. Fuji, T. Udem, A. Apolonski, F. Krausz, and T. W. Hänsch. Carrier envelope phase noise in stabilized amplifier systems. 30 (18), **2005**, 2487–2489.

[116] J. Rauschenberger, T. Fuji, M. Hentschel, A.-J. Verhoef, T. Udem, C. Gohle, T. W. Hänsch, and F. Krausz. Carrier-envelope phase-stabilized amplifier system. *Laser Physics Letters*, 3 (1), **2006**, 37–42. DOI: 10.1002/lapl.200510053.

[117] M. E. Fermann, V. I. Kruglov, B. C. Thomsen, J. M. Dudley, and J. D. Harvey. Self-similar propagation and amplification of parabolic pulses in optical fibers. *Physical review letters*, 84 (26 Pt 1), **2000**, 6010–3. URL: http://www.ncbi.nlm.nih.gov/pubmed/10991111.

[118] M. Hirano, T. Nakanishi, T. Okuno, and M. Onishi. Silica-Based Highly Nonlinear Fibers and Their Application. *Sel. Top. Quantum Electron.*, 15 (1), **2009**, 103–113. DOI: 10.1109/JSTQE.2008.2010241 (cited on page 12).

[119] D. Mandridis, I. Ozdur, F. Quinlan, M. Akbulut, J. J. Plant, P. W. Juodawlkis, and P. J. Delfyett. Low-noise, low repetition rate, semiconductor-based mode-locked laser source suitable for high bandwidth photonic analog – digital conversion. *Applied Optics*, 49 (15), **2010**, 2850–2857.

[120] H.-A. Bachor and P. J. Manson. Practical Implications of Quantum Noise. *Journal of Modern Optics*, 37 (11), **1990**, 1727–1740. DOI: 10.1080/09500349014551951.

[121] F. Quinlan, T. M. Fortier, H. Jiang, and S. a. Diddams. Analysis of shot noise in the detection of ultrashort optical pulse trains. *Journal of the Optical Society of America B*, 30 (6), **2013**, 1775. DOI: 10.1364/JOSAB.30.001775.

[122] D. C. Cole, K. M. Beha, S. A. Diddams, and S. B. Papp. Octave-spanning supercontinuum generation via microwave frequency multiplication. *Proceedings of the 8th Sympsion on Frequency Standards and Metrology 2015, Journal of Physics: Conference Series*, 723, **2016**, 012035. DOI: 10.1088/1742-6596/723/1/012035.

[123] A. M. Heidt. Efficient Adaptive Step Size Method for the Simulation of Supercontinuum Generation in Optical Fibers. *Journal of Lightwave Technology*, 27 (18), **2009**, 3984–3991 (cited on pages 9, 10).

[124] J. Hult. A Fourth-Order Runge-Kutta in the Interaction Picture Method for Simulating Supercontinuum Generation in Optical Fibers. *Journal of Lightwave Technology*, 25 (12), **2007**, 3770–3775. DOI: 10.1109/JLT.2007.909373 (cited on pages 9, 10, 12).

[125] R. Driad, J. Rosenzweig, R. E. Makon, R. Lösch, V. Hurm, H. Walcher, and M. Schlechtweg. InP DHBT-Based IC Technology for 100-Gb / s Ethernet. *IEEE Trans. on Electron. Devices*, 58 (8), **2011**, 2604–2609.

[126] D. Ferenci, M. Grozing, M. Berroth, R. Makon, R. Driad, and J. Rosenzweig. A 25 GHz Analog Demultiplexer with a Novel Track and Hold Circuit for a 50 GS / s A / D-Conversion System in InP DHBT Technology. In: **Microwave Symposium Digest**. 2012, pp. 1–3.

[127] K. J. Blow and D Wood. Theoretical description of transient stimulated Raman scattering in optical fibers. *Quantum Electronics, IEEE Journal of*, 25 (12), **1989**, 2665–2673. DOI: 10.1109/3.40655 (cited on page 12).